Influence of Structural and Topological Constraints on the Crystallization and Melting Behavior of Polymers: 3. Bisphenol A Polycarbonate

Azar Alizadeh,† Seungman Sohn,‡ Jeff Quinn, and Hervé Marand*

Departments of Chemistry and Materials Science and Engineering, Virginia Polytechnic Institute & State University, Blacksburg, Virginia 24061-0212

Leonard C. Shank and H. Darrell Iler

Department of Chemistry, Eastern Mennonite University, Harrisonburg, Virginia 22802-2462

Received August 14, 2000; Revised Manuscript Received March 19, 2001

ABSTRACT: In this paper, we report differential scanning calorimetry studies of the temperature and molar mass dependences for the primary and secondary crystallization behavior of bisphenol A polycarbonate (BAPC). The molar mass dependence of the crystallization rate is found to be much stronger during primary than during secondary crystallization, confirming our earlier claims that primary and secondary processes occur by significantly different mechanisms. Investigations of the secondary crystallization process suggest the existence of a crossover phenomenon from secondary crystal formation at low temperatures to isothermal lamellar thickening at high temperatures. While the results of our low-temperature studies of BAPC provide further support for the model developed in a previous publication on poly(arylene ether ether ketone), evidences from atomic force microscopy and calorimetry of isothermal lamellar thickening above the crossover temperature lead us to anticipate a more unified view of polymer crystallization.

Introduction

In the preceding two papers of this series, we reported investigations of the effect of topological constraints on the secondary crystallization of ethylene/1-octene random copolymers[1] (EO) and poly(arylene ether ether ketone)[2] (PEEK). Topological constraints in EO copolymers are structural in origin and associated with the quasi-random partitioning of each chain by hexyl branches. While the longest ethylene sequences between branch points are able to participate in the formation of primary chain-folded lamellae during the initial stage of cooling from the melt, the shorter sequences cannot do so and are thought to order in bundles or fringe-micellar-like secondary crystals when the temperature is further decreased. In the case of PEEK,[2] we conjectured that, as a result of chain stiffness effects, the lamellar growth process during primary crystallization is characterized by a low probability of adjacent or near-adjacent reentry folding. Irregular folding is believed to be at the source of a large population of cilia, loose folds, and tie chains. These amorphous sections of chains are pinned at lamellar surfaces as a result of primary crystallization and can subsequently achieve some level of crystallographic ordering only through local aggregation or clustering with neighboring chain segments. In contrast with EO copolymers, the "partitioning" process during the crystallization of PEEK is not thermodynamic in nature but arises from kinetic effects associated with the poor adjacent reentry folding expected for relatively stiff chains. Should this rather conceptual view of polymer crystallization have any merit, we anticipate very similar secondary crystallization characteristics in semiflexible chain polymers and in random copolymers, where co-units are excluded from the crystal lattice. While primary crystallization takes place from an unconstrained melt, secondary crystallization is associated with crystal formation from a conformationally constrained amorphous fraction, where the "constraints" originate from the primary crystals. In turn, these entropic differences may be at the origin of the dissimilarity in the kinetic laws associated with primary and secondary crystallization. For instance, the early stages of secondary crystallization in EO copolymers,[1] PEEK[2] and many other semicrystalline polymers[3] (such as PET, it-PP, s-PP, it-PS, and nylon-6) are characterized by an Avrami exponent of $^1/_2$. However, for these same polymers, the Avrami exponent associated with primary crystallization is in the usual range between 2 and 4.

Another systematic difference between primary and secondary crystals is found in their melting behavior. Upon heating EO copolymers, PEEK and other semicrystalline polymers (such as PET, PBT, it-PP, s-PP, it-PS, nylon-6, and ultrahigh molar mass polyethylene), a double melting behavior is usually observed. Under conditions where the lowest melting endotherm has specific characteristics (see below) and melting−recrystallization−remelting effects can be ruled out,[1,2,5] the multiple melting behavior can be explained in terms of a dual population of more stable (i.e., higher melting temperature) primary lamellar crystals and less stable (i.e., lower melting temperature) secondary crystals. The difference between the melting temperatures of primary and secondary crystals is believed to originate primarily in their morphology (different surface-to-volume ratios). In fact, bundlelike crystals usually melt at significantly lower temperatures than lamellae, even when both

* To whom correspondence should be addressed: hmarand@vt.edu.
† Current address: General Electric, CR&D, Niskayuna, NY 12309.
‡ Current address: LG Chemical Ltd, Taejon, Korea.

10.1021/ma001417s CCC: $20.00
Published on Web 05/11/2001

types of crystals are formed at the same temperature. During the past few years, we have studied the temporal evolution of endothermic transitions associated with the fusion of secondary bundlelike crystals. One of the strikingly similar features observed among many different polymers is the linear increase in the low endotherm peak position, T_m^{low} with the logarithm of crystallization time at a given crystallization temperature.[1−5] The slopes of these lines, denoted by $B(T_x)$, are found to decrease continuously with increasing temperature for all semicrystalline polymers investigated. The universality of these time and temperature dependences are discussed elsewhere.[3] It is sufficient to emphasize here that the above characteristics [Avrami exponent of $^1/_2$ and linear dependence of T_m^{low} vs $\log(t_x)$] can be regarded as signatures of secondary bundlelike crystallization.

In the present paper, we discuss the secondary crystallization of bisphenol A polycarbonate (BAPC). Two important characteristics of BAPC make this study particularly beneficial. First, fractionation of BAPC is relatively easy in comparison to that of other semiflexible polymers such as PEEK[4] or PET. Hence, BAPC is a good candidate for investigations of the effect of molar mass on the kinetics of secondary crystallization. Second, because of the extremely slow crystallization of BAPC,[6,7] primary and secondary stages can be more readily separated. Finally, in a recent publication,[5] we showed that the multiple melting behavior of this polymer is unequivocally explained in terms of the melting of separate populations of primary and secondary crystals. We also showed that melting−recrystallization−remelting effects, when present, are mostly observed in the high endothermic region and appear to be significant only for relatively low molar mass samples. In the present paper, we also address the effect of morphology prior to secondary crystallization on the kinetics of formation and the nature of secondary crystals. The initial polymer morphology is defined by several factors, such as the fraction of the lamellar crystals (or initial degree of crystallinity), the crystal thickness distribution and finally the distance between neighboring lamellae. In this respect, BAPC is again an excellent candidate for this particular study. For instance, we showed that selective or partial melting experiments on an initially semicrystalline BAPC, make it possible to obtain specimens which contain only high-melting (i.e., lamellar) crystals.[5] In this regard, a specific advantage offered by this polymer is the absence of further crystallization during fast cooling after partial melting.[5]

Until now, we have discussed secondary crystallization processes in terms of the formation of new crystals. It is important to mention that this is not the only conceivable mode of secondary crystallization. Indeed, it is well documented that secondary crystallization can also take place by a mechanism of isothermal lamellar thickening.[8] In the present paper, we establish the temperature window in which secondary crystallization of BAPC is explained by the formation of new crystals and examine the possibility of isothermal lamellar thickening at the highest crystallization temperatures. The concept of isothermal lamellar thickening has often been associated with that of the crystalline alpha relaxation process (α_C relaxation).[8,9] A very limited number of flexible semicrystalline polymers with short repeat units such as PE, it-PP, PEO, and PVDF exhibit an α_C relaxation (i.e., segmental motion within the crystal phase).[9,10] It is interesting to note that this relaxation is not expected in semiflexible polymers such as BAPC and PEEK since conformational motions within their crystalline phases are believed to require a significantly large activation energy.[9] The suggestion that isothermal lamellar thickening is possible in polymers such as BAPC brings up new perspectives and a possibly a more unified description of polymer crystallization.[3]

Table 1. Some of the Molecular Characteristics of the Bisphenol A Polycarbonate Samples Used in This Study (with Asterisks Indicating the Fractions)

sample designation	M_w ($g \cdot mol^{-1}$)	M_w/M_n	T_g (°C)[a]	ΔH_m^{total} ($J \cdot g^{-1}$)[b]
*BAPC-4K	4270	1.02	124.5	32.5
*BAPC-6K	6110	1.05	131.8	31.8
*BAPC-12K	12 400	1.10	137.8	28.0
*BAPC-17K	17 100	1.10	140.6	25.3
*BAPC-30K	29 800	1.20	146.1	NA
BAPC-19K	18 800	1.99	137.0	27.2
BAPC-28K	28 400	2.07	144.8	26.7

[a] Glass transition temperatures obtained after linear extrapolation to zero cooling rate. [b] Limiting (plateau) value of the total heat of fusion obtained after long crystallization times.

Experimental Section

The commercial bisphenol A polycarbonate (BAPC) samples investigated in the present work were manufactured by General Electric under the trade name of "Lexan" (IUPAC name poly(oxycarbonyloxy-1,4-phenyleneisopropylidene-1,4-phenylene)). Narrow molar mass distribution samples were obtained through fractionation of the highest molar mass commercial sample (BAPC-28K) (see below). The molar mass and polydispersity index of these commercial and fractionated materials were determined by GPC carried out in chloroform at 25 °C, using the absolute calibration method. The molecular characteristics of the commercial and fractionated samples used in the present study are collected in Table 1.

Fractionation Procedure. A solvent/nonsolvent fractionation method similar to those described by Schnell[11] and Sitaramaiah[12] was used. The procedure involves stepwise addition of methanol (nonsolvent) to a 0.5% w/v solution of BAPC in methylene chloride at 25.0 ± 0.1 °C. A 5 L round-bottom fractionation flask was modified through the addition of a 3 cm diameter by 5 cm long extension designed to amass the denser polymer-rich phases resulting from the successive stages of fractionation. For a given fraction, methanol was added dropwise with vigorous stirring until the solution develops a slight haze indicating a liquid/liquid-phase separation. After complete settling of the polymer-rich phase into the flask extension, the solvent-rich phase was siphoned off into a catch flask submerged in a 30.0 °C water bath. The polymer fraction was then collected by shocking with methanol and drying in a vacuum oven under reduced pressure at ambient temperature. Eleven fractions were obtained from 3 L of initial polymer solution. It should be noted that although the initial phase separation occurs by liquid−liquid demixing, crystallization was usually observed in the polymer-rich phase during the time allotted for settling. This actually made polymer collection easier and did not appear to adversely affect the efficiency of the fractionation procedure. Chemical degradation of polycarbonate during fractionation which was reported with this particular solvent/nonsolvent system[13,14] was minimized by using HPLC grade solvents stored under dry nitrogen blankets and by predrying each fraction under vacuum at temperatures below 25 °C.

Sample Preparation and Crystallization Procedures. The commercial samples provided in the form of pellets were purified by dissolution in chloroform and subsequent precipitation into methanol. These samples were washed several

times with HPLC grade methanol and then dried in a vacuum oven at 150 °C for a period of 24 h to remove any possible trace of solvent. To minimize the potential degradation of BAPC at high temperatures, which is induced by the presence of moisture, the commercial samples and fractions were further dried prior to crystallization for 24 h in a vacuum oven above their glass transition temperature and kept dry throughout the entire crystallization experiments. Amorphous films of 120 ± 20 μm thickness were prepared by compression molding of the dried samples at 250 °C and 150 psi under a nitrogen atmosphere for 5 min and subsequent cooling to room temperature. The amorphous films thus prepared were then wrapped in aluminum foil and placed in a temperature-controlled oven (fluctuations <±0.3 °C) at the desired crystallization temperature under an inert atmosphere. The samples were always crystallized by annealing from the glassy state.

GPC experiments carried out at different stages of sample preparation and crystallization indicate no change in sample molar mass distribution, thereby suggesting that degradation processes, if present, were insignificant.

Differential Scanning Calorimetry. The thermal behavior of BAPC samples was monitored by means of a model 2 Perkin-Elmer differential scanning calorimeter (DSC-2) operated with a homemade chiller bath. To reduce differences among samples due to thermal lag, discoid samples of 120 ± 20 μm thickness and 11.0 ± 1.0 mg weight were employed. Heating experiments were performed at different scanning rates ranging from 5 to 20 °C/min. The temperature calibration during heating was accomplished by recording the onset of the melting transition of an indium standard sandwiched between two amorphous BAPC films. Finally, isothermal crystallization experiments were carried out in the DSC cell, where the crystallization temperature, T_x, was calibrated by extrapolating the melting temperatures of standards (tin, lead and indium) to zero heating rate. In all cases, DSC traces are presented after subtraction of a baseline, which approximates the heat capacity of the semicrystalline sample over the temperature range considered. Therefore, the heating traces presented in this paper simply provide information on enthalpic changes associated with the melting process. As a result, the apparent heat capacities (dq/dT) vanish above and below the melting transition. Calorimetric glass transition temperatures were estimated at the inflection point of heat capacity traces, which were recorded during cooling at different scanning rates for fully amorphous samples. Temperature calibration of the DSC during cooling was achieved by recording the isotropic-to-nematic phase transition of *p*-azoxyanisole (T_{I-N} = 136.0 °C)). Note in Table 1 that glass transition temperatures increase by more than 25 °C over a decade change in molar mass.

Atomic Force Microscopy. Morphological studies were carried out using a Digital Instrument Dimension 3000 atomic force microscope (AFM). The AFM was operated in the tapping mode at room temperature using nanosensor TESP (tapping etched silicon probes) type single beam cantilevers. Images were collected in the phase mode. For this particular study, BAPC-28K lamellar crystals were grown edge-one under conditions of pseudo-epitaxy.[15] First, a 0.2% w/w polymer solution was prepared by dissolving BAPC-28K in HPLC grade chloroform. Next, several freshly cleaved calcite samples were immersed in the solution and removed after 1 min. The samples thus prepared were dried at 150 °C in *vacuuo* for a period of 24 h and then crystallized at 185 °C for 95 h. Finally, these samples were further annealed at 220 °C for different periods of time up to 18 h under inert atmosphere.

Results

Only very few publications have addressed the kinetics of crystallization of BAPC from the bulk at different temperatures.[16−18] Furthermore, to our knowledge, the effect of molar mass on the kinetics of bulk crystallization of BAPC has not been systematically studied. Therefore, we begin the Results section with

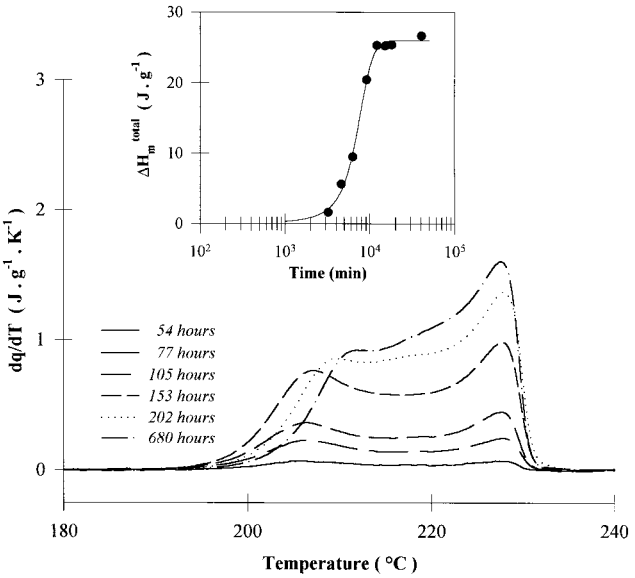

Figure 1. Heating traces (HR = 10 °C/min) of BAPC-28K crystallized at T_x = 185 °C for times ranging from 54 to 680 h. Inset shows the corresponding temporal evolution of the total heat of fusion.

investigations of the overall kinetics of bulk crystallization of BAPC of varying molar mass. From our previous study, we know that the overall kinetics of crystallization reflects both primary and secondary crystal formations.[5]

I. Overall Kinetics of Crystallization. In Figure 1, the melting traces of BAPC-28K crystallized at 185 °C for different periods of time are displayed. The choice of BAPC-28 here is arbitrary as other polycarbonate samples display a qualitatively similar behavior. BAPC-28K exhibits a multiple melting behavior upon heating after isothermal crystallization at 185 °C. While the location of the higher melting endotherm is independent of crystallization time, the melting temperature associated with the lower endotherm shifts continuously to higher values with increasing crystallization time. The total enthalpy of fusion (including both the low and the high endotherms), ΔH_m^{total}, was determined for each crystallization time from the area under the DSC curve between the fixed limits of 160 and 250 °C. We note that the ratio of the low to high endotherm enthalpies is approximately independent of crystallization time. The insert in Figure 1 shows the variation of ΔH_m^{total} with crystallization time for BAPC-28K crystallized at 185 °C. We also note that a significant induction period (≈40−50 h) is required for the detection of the first signs of crystallinity at this temperature. As observed in the inset figure, after an induction period, ΔH_m^{total} increases steeply at first and much more slowly at the longest crystallization times. Similar experiments were performed with each of the bisphenol A polycarbonate samples at a variety of crystallization temperatures. Approximate limiting crystallinities estimated for the various samples at long crystallization times are in the range 22−28%.

First, let us focus on the crystallization temperature dependence of ΔH_m^{total} for BAPC-4K. The choice of BAPC-4K as an example stems from its widest crystallization window among all samples investigated. Figure 2 depicts the temporal evolution of ΔH_m^{total} of BAPC-4K at different crystallization temperatures. The induction period for the detection of any traces of crystallinity

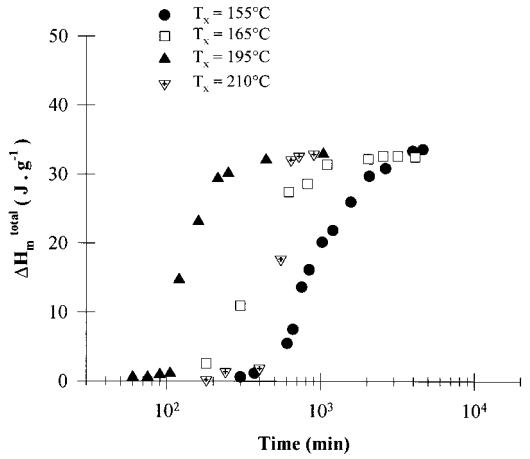

Figure 2. Temporal evolution of the total heat of fusion of BAPC-4K at different crystallization temperatures.

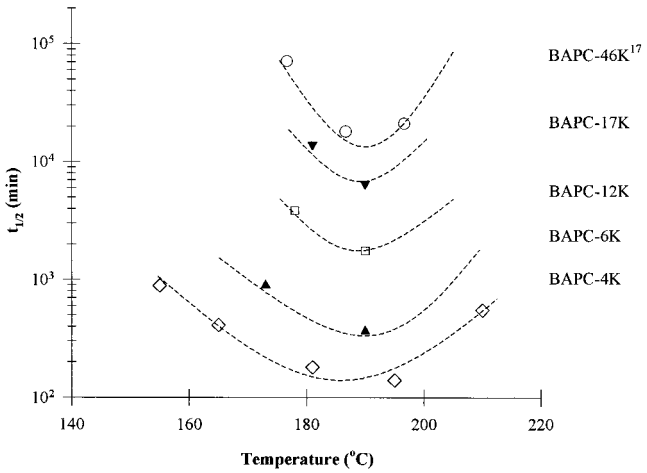

Figure 3. Variation of the half time of crystallization of BAPC samples as a function of crystallization temperature. Open circle: data from ref 17. Other symbols: this work.

is clearly temperature dependent. In contrast, the apparent limiting value of the heat of fusion is virtually independent of crystallization temperature. A similar qualitative temperature dependence of ΔH_m^{total} is observed for the other commercial and fractionated BAPC samples. It should be emphasized again that the apparent induction period and to a lesser extent the limiting value of ΔH_m^{total} are molar mass dependent. The limiting values of ΔH_m^{total} are collected in Table 1. An accurate determination of the apparent induction period for each temperature and molar mass would require significant data collection at the early stages of crystallization and was not attempted. The half-time of crystallization, $t_{1/2}$, however, can be defined with a higher level of accuracy, as the time elapsed to achieve half of the limiting value of ΔH_m^{total}. In Figure 3, $t_{1/2}$ is plotted as a function of crystallization temperature for different BAPC samples. In this figure we have also included the half times of crystallization reported in the literature for an other commercial polycarbonate sample (M_w = 46 000 g·mol^{-1}).[17] The dotted lines in this figure are not curve fits but simple guides to the eye. From Figure 3, we conclude that the observable crystallization window for bisphenol A polycarbonate becomes narrower with increasing molar mass. This apparent narrowing of the crystallization window is possibly a consequence of a stronger effect of chain length on segmental mobility than on crystallization driving force.

Table 2. Conditions for Crystallization and Partial Melting of BAPC Samples Prior to the Secondary Crystallization Experiments

sample designation	crystallization conditions	partial melting (PM) (°C)
BAPC-4K	165 °C, for 38 h	216
BAPC-6K	173 °C, for 49 h	215
BAPC-12K	178 °C, for 160 h	220
BAPC-17K	181 °C, for 382 h	217
BAPC-19K	170 °C, for 384 h	217
BAPC-28K	185 °C, for 202 h	220

We also note that the $t_{1/2}$ vs crystallization temperature curves exhibit a minimum around T_x = 190 °C, approximately independent of molar mass.

II. Secondary Crystallization. Secondary crystallization experiments can be divided into two main groups according to the crystallization temperature range over which they are conducted.

II-1. Low Crystallization Temperature Region. For a given polycarbonate sample, the "low" secondary crystallization temperature region encompasses a temperature range between its glass transition temperature, T_g, and a crossover temperature, T_{CO}, which will be defined later in the discussion section. Two types of experiments are presented in this section: (1) For a given sample and secondary crystallization temperature, the role played by the initial morphological state was probed. (2) The effects of crystallization temperature, molar mass, and heating rate on the kinetics of secondary crystallization and melting behavior of BAPC were investigated. In both types of experiments, isothermal secondary crystallization was conducted after partial melting of samples that had been crystallized from the glassy state according to the specifications of Table 2. The choice of specific crystallization conditions (temperature and time) was based on the results of the overall kinetics of crystallization presented in the preceding section.

II-1-a. Effect of the Initial Morphology. As mentioned in the Introduction, by varying the crystallization conditions employed to obtain the initial semicrystalline BAPC, on one hand, and the temperature of partial melting, on the other hand, one can tailor the environment for the formation of secondary crystals. In this set of experiments, samples BAPC-19K and BAPC-28K were examined. Typical results are presented for BAPC-28K.

BAPC-28K was crystallized by annealing from the glass at a temperature of 185 °C for a period of 202 h (BAPC-28K; 202 h in Table 2). This sample was then partially melted (PM) by heating at a rate of 40 °C/min to a temperature above the low endotherm (T_{PM} = 220 °C) and kept at that temperature for 1 min. The heats of fusion of the original and partially melted samples are 25.4 and 8.3 J/g, respectively. After partial melting, the sample was quenched at the maximum cooling rate available with the DSC-2 to the secondary crystallization temperature, T_x = 185 °C, and maintained at that temperature for a given period of time, t_x. The sample was then quenched to room temperature and its heating trace was recorded at a rate of 10 °C/min. This procedure was repeated for different secondary crystallization times. In Figure 4 we show typical heating traces for this set of samples for times ranging from 5 to 900 min. Also plotted in this figure is the melting trace of a partially melted sample, which was not subjected to

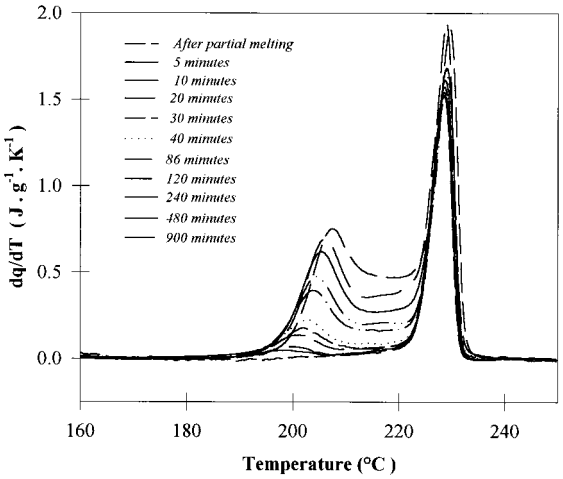

Figure 4. Heating traces (HR = 10 °C/min) of BAPC-28K 202 h after partial melting at T_{PM} = 220 °C and secondary crystallization at T_x = 185 °C for times ranging from 5 to 900 min.

further crystallization at 185 °C. As a result of the *second* isothermal crystallization at 185 °C, a low endothermic peak is observed just above this temperature during the subsequent heating. Similarly, secondary crystallization experiments were performed at 185 °C on two other BAPC-28K samples, which were initially cold crystallized at 185 °C for shorter times (105 and 153 h, respectively). These samples, designated (BAPC-28K; 105 h) and (BAPC-28K; 153 h), exhibited overall heats of fusion of 9.5 and 20.4 J·g^{-1}, respectively. After partial melting at T_{PM} = 220 °C, their heats of fusion decrease to 2.7 and 5.9 J·g^{-1}, respectively. Melting traces of these last two samples, after partial melting and secondary crystallization, show very similar features to those shown in Figure 4 for (BAPC-28K; 202 h).

We now focus on the quantitative analysis of the time dependence of the melting temperature, T_m^{low}, and the heat of fusion, ΔH_m^{low}, associated with the low endotherm for samples (BAPC-28K; 105 h), (BAPC-28K; 153 h), and (BAPC-28K; 202 h), resulting from secondary crystallization at 185 °C. In Figure 5a, T_m^{low} is found to increase linearly with $\log(t_x - t_0)$ over more than four decades, where t_0 is an apparent induction period, defined as the time required to detect a measurable heat of fusion (≥0.4 J·g^{-1}) for the low endotherm. Under these conditions, the induction periods for (BAPC-28K; 105 h), (BAPC-28K; 153 h), and (BAPC-28K; 202 h) are reproducibly found to be 7, 3, and 2 min, respectively, as opposed to nearly 40−50 h for the original BAPC sample. The filled symbols in Figure 5a correspond to the low endotherm peak temperature for the original samples at different stages of crystallization. Note that the data scatter is larger in this case than for samples undergoing secondary crystallization after partial melting. Such a scatter results from the overlap between the low and high endotherms at very long crystallization times (see the heating traces of original samples in Figure 1). As mentioned above, an apparent induction period of about 45 h is required to detect any trace of crystallinity during the cold-crystallization of BAPC-28K. Once this induction time is accounted for, we find the important result that *the same* T_m^{low} vs $\log(t_x)$ dependence is exhibited by all samples (see Figure 5a).

Following the formalism used in the preceding papers,[1−3] the variation of T_m^{low} with $\log(t_x)$ is expressed

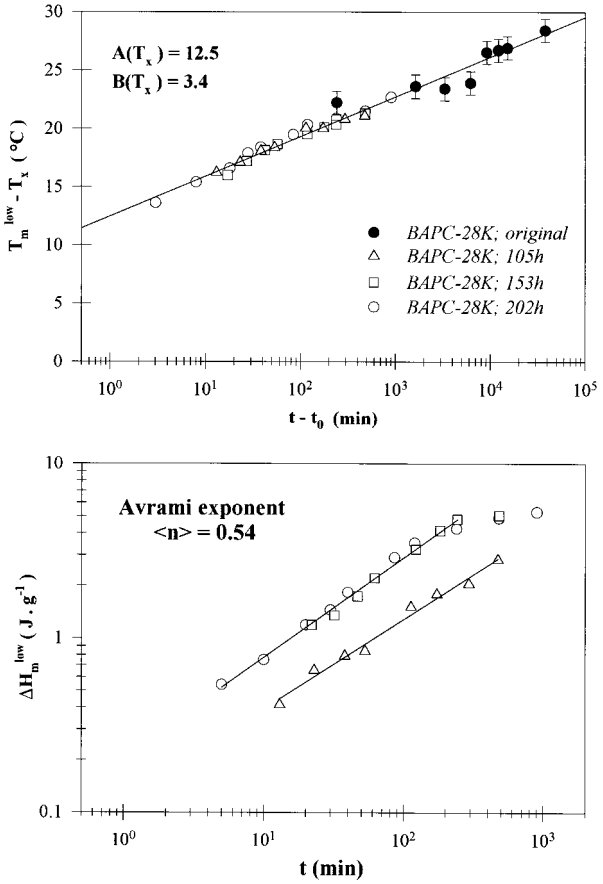

Figure 5. Effect of the initial level of crystallinity on the temporal evolution of (a) melting peak temperatures and (b) enthalpies of fusion of the low endotherm in BAPC-28K. Secondary crystallization and partial melting conditions are identical with those in Figure 4.

empirically by

$$T_m^{low} = T_x + A(T_x) + B(T_x)\log(t_x) \qquad (1)$$

The best fit parameters $A(T_x)$ and $B(T_x)$ for BAPC-28K at T_x = 185 °C are given in Figure 5a. We also use the same formalism as described in our earlier papers to analyze the heat of fusion associated with the low endotherm. In this context, adopting the free-growth approximation,[19] we write the crystallization time dependent heat of fusion as

$$\Delta H_m^{low} = K t_x^{\,n} \qquad (2)$$

Plots of $\log(\Delta H_m^{low})$ as a function of $\log(t_x)$ for (BAPC-28K; 105 h), (BAPC-28K; 153 h), and (BAPC-28K; 202 h) shown in Figure 5b are linear at the early stages of secondary crystallization. Their slopes are identified with the Avrami exponent, n, which characterizes the geometry and the mechanism of growth. K is proportional to the rate of secondary crystallization at the early stage. Data in Figure 5b indicate that the initial stage of secondary crystallization is characterized by an Avrami exponent in the vicinity of $^1/_2$. At later stages of secondary crystallization, ca. 100−200 min, a deviation from linearity is observed, indicating that ΔH_m^{low} continues to increase with time but at a much slower rate.

Similar experiments were conducted for the BAPC-19K sample. In this case, the initial cold crystallization

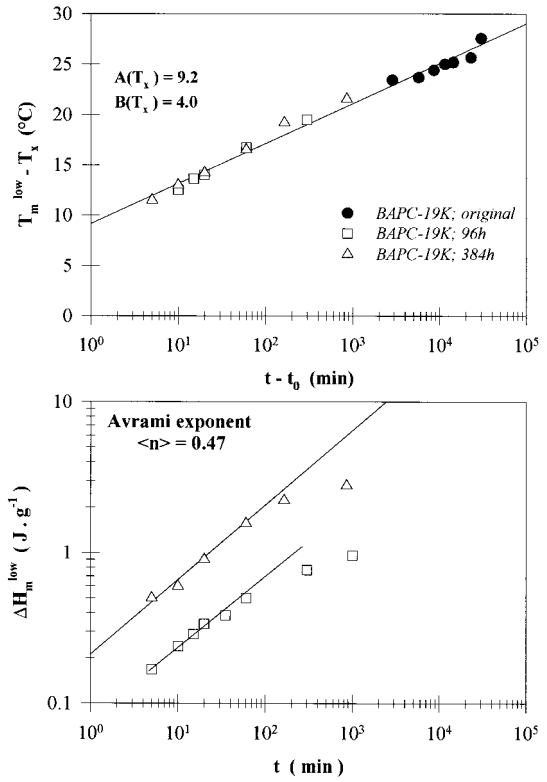

Figure 6. Effect of the initial level of crystallinity on the temporal evolution of (a) melting peak temperatures and (b) enthalpies of fusion of the low endotherm in BAPC-19K. Partial melting and secondary crystallization were conducted at 217 and 170 °C, respectively.

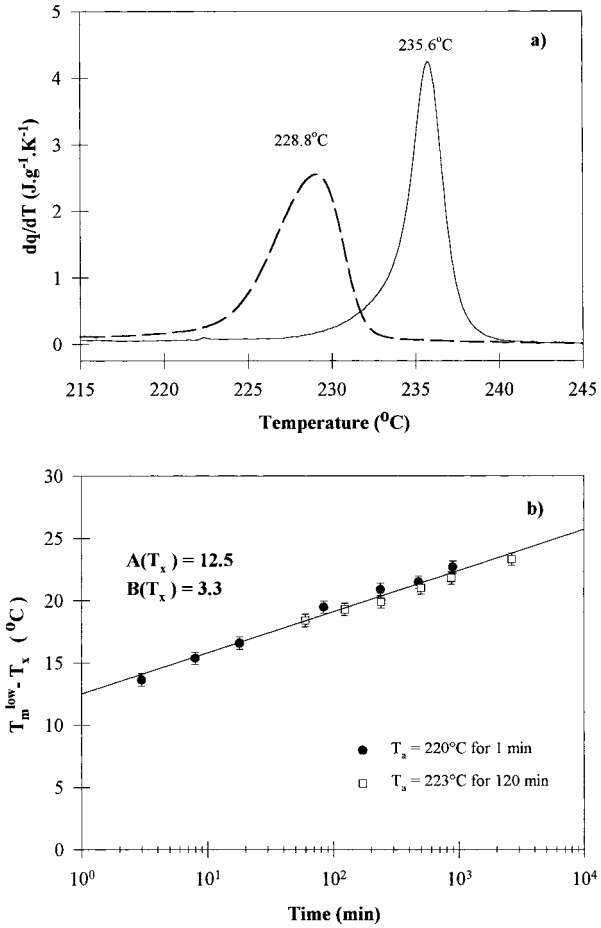

Figure 7. Effect of the initial morphology on the kinetics of secondary crystallization. (a) Melting traces of BAPC-28K prior to secondary crystallization. The dashed curve represents the sample cold-crystallized according to the conditions depicted in Table 2 and then annealed at 220 °C for 1 min, while the solid curve corresponds to the sample annealed at 223 °C for 120 min. (b) Temporal evolution of T_m^{low} after secondary crystallization at 185 °C.

was performed at 170 °C for 96 and 384 h. Partial melting was carried out at T_{PM} = 217 °C, and the secondary crystallization stage was performed at 170 °C for times ranging from 1 to 1000 min. The temporal evolutions of T_m^{low} and ΔH_m^{low} are displayed in Figure 6, parts a and b, for this series of samples. These plots, once more, demonstrate the linear variation of T_m^{low} vs $\log(t_x)$ and an Avrami exponent of $^1/_2$ for the initial stage of secondary crystallization. We note that for both BAPC-19K and BAPC-28K, the absolute magnitude of ΔH_m^{low} appears to depend on the initial degree of crystallinity (heat of fusion) of the sample after partial melting. In other words, a sample with a lower heat of fusion after partial melting (BAPC-28K; 105 h in this case) (i.e lower initial degree of crystallinity) will also exhibit a lower value of ΔH_m^{low} (i.e., a lower extent of secondary crystallization). The apparent overlap between BAPC-28K 153 and 202 h samples may be due to a lack of sensitivity in our measurements and to the fact that the initial degrees crystallinity are not significantly different (see Figure 1).

The previous series of experiments suggest the influence of the initial level of crystallinity (fraction of lamellar type crystals) on the kinetics of secondary crystallization. The initial morphology can also be modified by varying the lamellar thickness of primary crystals. In this context, we present the results of secondary crystallization for two BAPC-28K samples, which exhibit different lamellar thicknesses and possibly different long-spacings prior to secondary crystallization. In Figure 7a the melting traces of the initial samples (prior to secondary crystallization) are displayed. Details of the experimental conditions for the preparation of these samples are indicated in the legend to Figure 7. Although their peak melting temperatures differ by almost 7 °C, their heats of fusion are very similar. We note that differences in peak melting temperature simply reflect differences in lamellar thickness. Secondary crystallization experiments were performed at 185 °C for various periods of time. Heating traces recorded after the above thermal treatments reveal the presence of a low endotherm whose corresponding heat of fusion and melting temperature increase with secondary crystallization time. The temporal evolution of T_m^{low} for both sets of samples is depicted in Figure 7b. For a given t_x, and within experimental uncertainty, T_m^{low} is independent of the lamellar thickness prior to secondary crystallization. Similar experiments conducted on BAPC-19K lead us to draw the same conclusion.

II-1-b. Effect of Crystallization Temperature. In this series of experiments, several amorphous samples were cold-crystallized under the conditions given in Table 2 to ensure spherulitic impingement. These samples were partially melted at T_{PM} (Table 2) and subsequently quenched at the maximum cooling rate available to the crystallization temperature, T_x, at which they were kept for a given time, t_x. Such samples were then quenched to room temperature and immediately reheated to record their melting behavior. The nomen-

Table 3. Parameters Describing the Temporal Evolution of the Low Endotherm for Various BAPC Samples at Different Secondary Crystallization Temperatures: Effects of Crystallization Temperature and Molar Mass

BAPC-28K	$A(T_x)$	$B(T_x)$	K	n
$T_x = 165$ °C	13.4	4.3	0.06	0.59
$T_x = 175$ °C	12.5	4.2	0.19	0.53
$T_x = 185$ °C	12.3	3.6	0.27	0.52
$T_x = 195$ °C	11.5	3.3	0.30	0.66
BAPC-12K	$A(T_x)$	$B(T_x)$	K	n
$T_x = 168$ °C	9.0	4.5		
$T_x = 178$ °C	9.7	3.8	0.32	0.54
$T_x = 183$ °C	8.4	3.9		
BAPC-6K		$A(T_x)$		$B(T_x)$
$T_x = 163$ °C		6.7		4.6
$T_x = 173$ °C		8.6		3.0
$T_x = 178$ °C		8.6		2.7
BAPC-4K		$A(T_x)$		$B(T_x)$
$T_x = 155$ °C		4.9		5.7
$T_x = 165$ °C		8.7		3.6
$T_x = 170$ °C		8.1		3.5

clature (BAPC-XX; PM-T_{PM}; SC-T_x) describes a given secondary crystallization experiment, where BAPC-XX provides identification of the sample molar mass and the initial crystallization conditions (Table 2), PM-T_{PM} specifies the temperature at which partial melting was carried out, and SC-T_x designates the temperature for the second crystallization stage. For instance, (BAPC-28K; PM-220; SC-175) implies that the sample BAPC-28K, initially crystallized at 185 °C for 202 h, was partially melted at 220 °C and further crystallized at 175 °C.

Analysis of heating traces after secondary crystallization provides access to the crystallization time dependence of the melting temperature and heat of fusion associated with the low endotherm. These quantities were in turn analyzed using eqs 1 and 2 to yield the parameters $A(T_x)$, $B(T_x)$, K, and n (see Table 3). The values of the K and n parameters are not included for BAPC-4K and BAPC-6K, since a rigorous analysis of the enthalpy associated with the low endotherm could not be performed for short crystallization times. Indeed, low molar mass samples, which are only allowed to crystallize for short times under isothermal conditions, can develop further crystallinity during the subsequent heating. The exotherm associated with crystallization during heating unfortunately overlaps the low endotherm associated with the melting of secondary crystals formed at T_x. This is, however, not an issue for longer secondary crystallization times, since the rate of secondary crystallization decreases with time beyond the initial stage, and the crystallinity developed during heating becomes negligible. The parameters $A(T_x)$ and $B(T_x)$ reported for samples BAPC-4K and BAPC-6K in Table 3 are thus derived from measurements on samples crystallized for long times. Crystallization during heating is not expected for higher molar mass BAPC samples, since the rate of crystallization decreases with increasing chain length for these materials. For all BAPC samples, an increase in crystallization temperature results in a decrease in the slope $B(T_x)$ (see Table 3). A direct comparison of the $B(T_x)$ values for the different samples is not possible, since $B(T_x)$ is strongly heating rate dependent[3,5] and, more importantly, the heating rate dependence is not universal, but it is shown

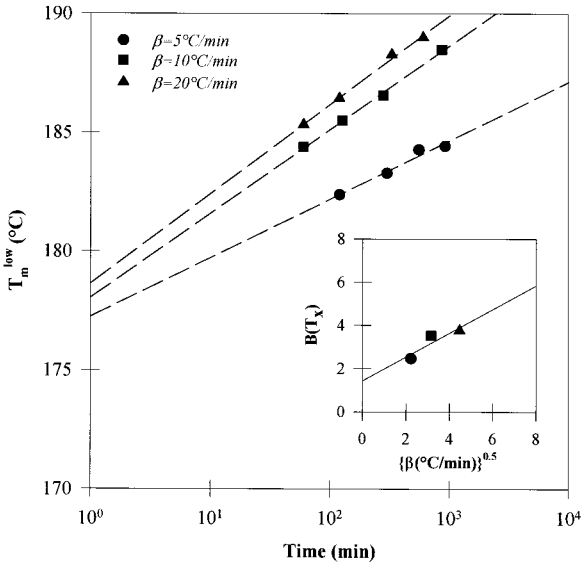

Figure 8. Temporal evolution of the low endotherm melting temperature in BAPC-4K crystallized at $T_x = 165$ °C at different heating rates. The inset shows the rate of shift of the low endotherm as a function of square root of heating rate.

Table 4. Parameters Describing the Temporal Evolution of the Low Endotherm for Various BAPC Samples at Secondary Crystallization Temperatures below T_{CO}: Effect of Heating Rate

	$T_x = 155$ °C		$T_x = 165$ °C		$T_x = 170$ °C	
BAPC-4K	$A(T_x)$	$B(T_x)$	$A(T_x)$	$B(T_x)$	$A(T_x)$	$B(T_x)$
$\beta = 20$ °C/min	5.8	5.7	7.3	4.3	8.7	3.8
$\beta = 10$ °C/min	5.8	5.4	7.1	3.6	8.1	3.5
$\beta = 5$ °C/min	5.9	4.2	6.6	3.0	7.3	2.5
$\beta = 0$ °C/min	6.0	2.9	6.0	1.9	6.0	1.4

	$T_x = 165$ °C		$T_x = 175$ °C		$T_x = 185$ °C		$T_x = 195$ °C	
BAPC-28K	$A(T_x)$	$B(T_x)$	$A(T_x)$	$B(T_x)$	$A(T_x)$	$B(T_x)$	$A(T_x)$	$B(T_x)$
$\beta = 20$ °C/min	10.7	5.3	11.1	4.6	10.2	3.9	11.6	4.3
$\beta = 10$ °C/min	10.2	5.2	10.9	4.2	11.7	3.9	11.3	3.3
$\beta = 5$ °C/min	8.0	4.3	8.6	3.6	9.3	3.0	9.8	2.8
$\beta = 0$ °C/min	5.8	3.6	6.7	2.8	9.4	2.1	8.4	1.3

below to vary with molar mass. The effect of heating rate on the magnitude of the slope $B(T_x)$ was investigated for the two extreme molar masses, i.e., samples BAPC-4K and BAPC-28K. For each sample, secondary crystallization experiments were performed at several temperatures, T_x, and the subsequent melting behaviors were examined at heating rates ranging from 5 to 20 °C/min. The results of such analyses (Table 4) indicate that, at all heating rates, $B(T_x)$ decreases linearly with increasing T_x. For a given BAPC sample and at a constant T_x, $B(T_x)$ is found to increase with heating rate. This is depicted more clearly in Figure 8, where the temporal evolution of T_m^{low} is illustrated for different heating rates in the case of BAPC-4K after secondary crystallization at $T_x = 165$ °C. As seen in this figure, the slopes $B(T_x)$ become larger with increasing heating rate, β. In a previous paper, we discussed the heating rate dependence of the parameters $A(T_x)$ and $B(T_x)$ in relation to superheating of secondary crystals during melting.[3,5] As a result of superheating, T_m^{low} and, thus, $B(T_x)$ increase linearly with the square root of heating rate for given crystallization conditions. The inset of Figure 8 depicts the variation of $B(T_x)$ as a function of the square root of heating rate, $\beta^{0.5}$. The linear extrapolation of $B(T_x)$ vs $\beta^{0.5}$ to zero heating rate provides an adequate correction for superheating effects, thus

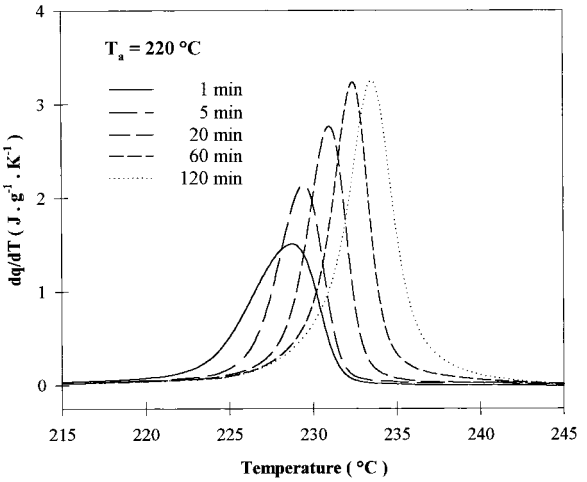

Figure 9. Heating traces (HR = 10 °C/min) of BAPC-28K exposed to isothermal annealing at 220 °C for varying times. (Prior to annealing, the samples were crystallized according to the conditions depicted in Table 2.)

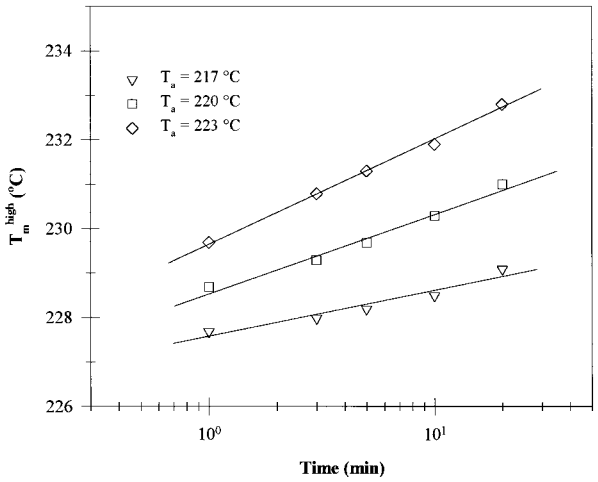

Figure 10. Temporal evolution of the high endotherm melting temperature in BAPC-28K samples exposed to annealing at high temperatures.

yields the *intrinsic rate of shift of the low endotherm*, $[B(T_x), \beta \rightarrow 0]$, for a given crystallization temperature. It is important to mention again that the degree of superheating is a function of the molecular structure of the polymer (molar mass, chain stiffness), the crystallization and also the melting conditions. Therefore, to compare different polymers (or BAPC of different molar masses in the present case), one needs to determine the intrinsic rate of shift of the low endotherm $[B(T_x), \beta \rightarrow 0]$. We have included in Table 4 the values of $[B(T_x), \beta \rightarrow 0]$ for the two BAPC investigated at different crystallization temperatures.

II-2. High Crystallization Temperature Region. This region of secondary crystallization encompasses a temperature range between the crossover temperature, T_{CO}, and the ultimate melting point of the sample. Secondary crystallization experiments in the high-temperature region were performed on the two extreme molar mass samples, BAPC-4K and BAPC-28K. Once again we show the results of such experiments for BAPC-28K for illustration purpose. A series of samples were cold-crystallized under the conditions depicted in Table 2 (185 °C for 202 h) and then annealed isothermally inside the DSC cell at temperatures above 210 °C for times ranging from 1 to 120 min. Analysis of longer annealing time experiments is not included here to avoid complications due to chemical degradation effects and extensive formation of new primary lamellae. After crystallization, the samples were cooled at the maximum rate available to 100 °C, and heating traces were then recorded at 10 °C/min. In Figure 9, heating traces of BAPC-28K are displayed after annealing at 220 °C between 1 and 120 min. Most remarkably, a single melting endotherm is observed for all annealing times. Similar results are obtained for all annealing experiments in the high-temperature region. This behavior must be contrasted with that observed in the low-temperature region, where isothermal secondary crystallization always results in a multiple melting behavior upon heating. Examination of Figure 9 also shows a continuous shift of the melting endotherm toward higher temperatures with increasing annealing time. In Figure 10, the melting temperature, T_m^{high}, is plotted as a function of logarithm of time for several annealing temperatures. T_m^{high} increases linearly with $\log(t_x)$. The slopes of these lines have been also represented by the symbol $B(T_x)$. The values of $B(T_x)$ corresponding to the different annealing temperatures (in the high-temperature region) are collected in Table 5. Note that for both molar masses investigated, $B(T_x)$ increases with increasing annealing temperature. This trend is thus opposite to that observed in the low crystallization temperature region (see Tables 3 and 4).

Table 5. Parameters Describing the Temporal Evolution of the Low Endotherm for Various BAPC Samples at Secondary Crystallization Temperatures above T_{CO}

	T_x = 195 °C		T_x = 200 °C		T_x = 205 °C	
BAPC-4K	$A(T_x)$	$B(T_x)$	$A(T_x)$	$B(T_x)$	$A(T_x)$	$B(T_x)$
β = 10 °C/min		0.7		1.0		1.2
	T_x = 217 °C		T_x = 220 °C		T_x = 223 °C	
BAPC-28K	$A(T_x)$	$B(T_x)$	$A(T_x)$	$B(T_x)$	$A(T_x)$	$B(T_x)$
β = 10 °C/min	10.6	1.1	8.6	1.8	6.7	2.3

Discussion

Overall Kinetics of Crystallization. When comparing the kinetics of crystallization of different semicrystalline polymers, it is important to do so at a constant degree of undercooling; i.e., the difference between the equilibrium melting point and the crystallization temperature should be kept constant.[8,20] This practice is however rarely followed rigorously since equilibrium melting temperatures are often elusive quantities. Even though estimates of the equilibrium melting temperature of bisphenol A polycarbonate have been proposed, the variation of this thermodynamic property with chain length is not available. The equilibrium melting temperature of a polymer crystal phase may be estimated through either the nonlinear Hoffman−Weeks analysis or the Gibbs−Thompson approach only when the chain length is sufficiently large.[21] In the particular case of BAPC, the crystallization window is extremely narrow,[11,17] thus making both extrapolative procedures unreliable.

Since at this moment we cannot strictly adhere to the criterion of constant undercooling, we have opted to compare the kinetics of crystallization of the different polycarbonate samples at the corresponding minima of their $t_{1/2}$ vs T_x plots. As seen in Figure 3, the temperature at maximum crystallization rate appears to be

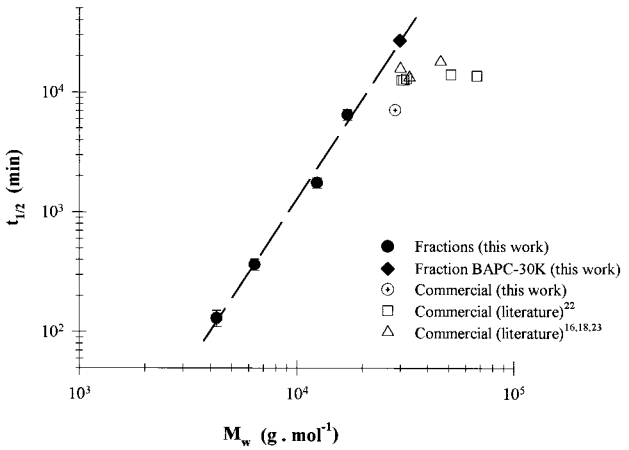

Figure 11. Variation of the half time of crystallization of fractionated and commercial BAPC as a function of weight-average molar mass (BAPC-30K was crystallized for 430 h at 185 °C and a crystallinity of 1% was measured; thus, this point does not correspond to the half time).

independent of molar mass. Other studies[6,16−18] in the literature yielded similar results and a temperature of 190 °C is often reported to correspond to the maximum rate of crystallization of BAPC. In Figure 11, $t_{1/2}$ of several BAPC samples obtained around 190 °C are plotted as a function of their average molar mass. The crystallization half time increases steeply with molar mass for the fractions (filled symbols), following a $t_{1/2} \propto M^{2.8}$ power law over the molar mass range available for the BAPC fractions.[22] For the fraction characterized by $M_w = 30\,000$ g·mol^{-1}, only 1% crystallinity was obtained after extremely long crystallization times (450 h). In contrast, the commercial sample BAPC-28K (crossed symbol) with a very similar molar mass, not only crystallizes much faster, but also develops a significantly higher level of crystallinity (≈25%) for similar crystallization times. In Figure 11, the half times reported in the literature for the crystallization of other commercial BAPC samples have also been included (open symbols).[16,23,24] The values of $t_{1/2}$ obtained in this study for the commercial samples are in excellent agreement with the literature data. Furthermore, we note that $t_{1/2}$ becomes independent of chain length for polydisperse specimens when $M_w > 20\,000$ g·mol^{-1}. An explanation for the faster crystallization of polydisperse samples is proposed next. Comparing a commercial material (polydispersity index of ca. 2.0) and a fraction of identical weight-average molar mass, the former material contains a much more sizable fraction of short chains than the latter. Our study of the fractions indicates that, for the range of molar masses investigated, the rate of crystallization decreases with increasing chain length at a fixed crystallization temperature. This indicates that chain length affects more significantly the segmental transport contribution to the crystallization rate (in both nucleation and growth processes) than the secondary nucleation rate. Whether this observation can be explained by the effect of chain length on either the width of the crystallization window ($T_m - T_g$ difference) or the activation energy for self-diffusion as in the case of PEO[25] or even both cannot be ascertained at the present time and will require further study. Returning to the polydispersity effect discussed above, we find only a weak dependence of the limiting crystallinity on chain length for polydisperse samples. This observation is possibly explained by the fact that short chains may act as diluents for the longer chains, thereby increasing the rate at which long chains crystallize in the polydisperse sample. The crystals formed by the shorter chains may also act as nucleation sites for the longest chains, thus increasing the fraction of material that can crystallize in a given time.

Bisphenol A polycarbonate exhibits a slower kinetics of crystallization and a narrower crystallization window ($T_m - T_g$) than semicrystalline polymers like PEEK, PPS, PET, and PBT but not significantly different from that of it-PS, if the literature values of the equilibrium melting temperature are to be trusted.[21] A further reason for the slow kinetics of crystal growth of BAPC may be proposed on the basis of secondary nucleation arguments.[26] Estimates of the work of chain folding for BAPC (27.3 kcal/mol of fold vs 5.7 for polyethylene)[6] suggest that the rates of secondary nucleation and lateral substrate completion would be extremely low.[26] It is not clear, however, that such concepts are rigorously applicable to semiflexible chain polymers, as the extent of adjacent reentry folding may be extremely low in this case. Further evidence that segmental motion controls the rate of BAPC crystallization is gained from the observed enhancement in crystallization rate when this materials is exposed to solvents or vapors.[6,27,28]

Secondary Crystallization. In the Results section, we claimed that two regimes of secondary crystallization are distinguishable for BAPC. We first establish the crossover temperature between these two regimes. Next, we propose an explanation for the different mechanisms of secondary crystallization in each of these temperature ranges and for the crossover phenomenon.

Crossover Temperature, T_{CO}. By investigating the melting behavior of BAPC samples after different secondary crystallization histories, we obtained the intrinsic rates of shift of the melting endotherm to higher temperatures with logarithm of time (see $[B(T_x), \beta\rightarrow 0]$ in Tables 4 and 5). In the "low temperature region", the shift is observed solely for the lower endotherm. In the "high temperature region", $[B(T_x), \beta\rightarrow 0]$ represents the shift in the melting temperature associated with the only endotherm present. The observation that $[B(T_x), \beta\rightarrow 0]$ is always positive, is consistent with the thermodynamic argument that, at the crystallization temperature, the difference in free energy between the crystal and the amorphous fractions increases with time. The observation that $[B(T_x), \beta\rightarrow 0]$ has opposite temperature dependences in the low and high-temperature regions (Figure 12a) suggests the existence of two different mechanisms for the relative stabilization of the crystal fraction over the amorphous fraction. Examination of Figure 12a indicates that $[B(T_x), \beta\rightarrow 0]$ exhibits its highest value at low crystallization temperatures, (i.e., closer to T_g) and decreases approximately linearly with temperature. Linear extrapolation of $[B(T_x), \beta\rightarrow 0]$ to zero allows us to define the crossover temperature, which we denote T_{CO}. Above the crossover temperature, i.e., in the high-temperature region, $[B(T_x), \beta\rightarrow 0]$ increases linearly with temperature. It is important to notice that the two lines describing the variation of $[B(T_x), \beta\rightarrow 0]$ vs T_x intersect the temperature axis at the same location, i.e., at the crossover temperature. As shown in Figure 12b, the low molar mass sample (BAPC-4K) exhibits a very similar behavior, with a crossover temperature, $T_{CO} \approx 187$ °C.

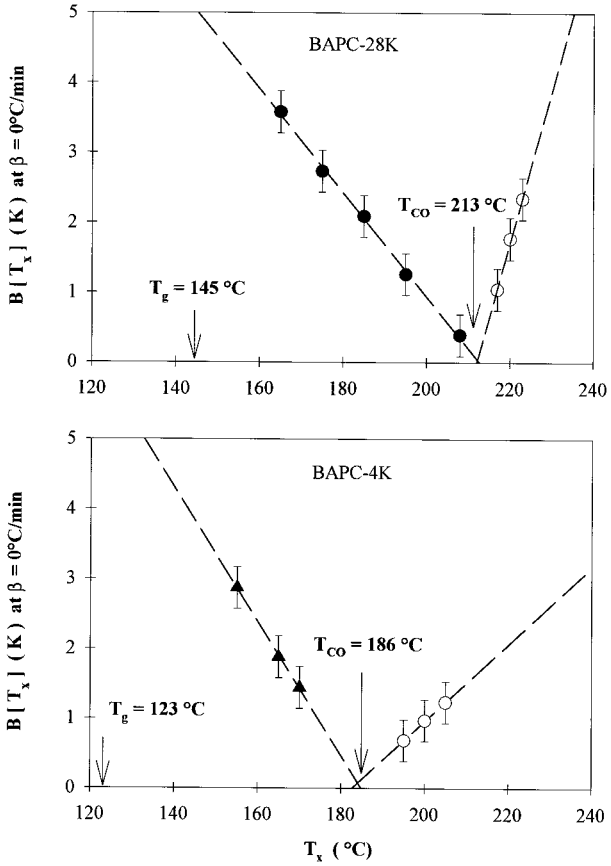

Figure 12. Variation of $B(T)$ at zero heating rate as a function of T_x: (a) BAPC-28K and (b) BAPC-4K.

Note that the crossover temperature for BPAC-4K is below that of BAPC-28K. Similar plots have also been recently obtained in our laboratory for other semicrystalline polymers, such as PEEK, it-PS, and PET.[3] Although the crossover temperature is found to depend on chain structure and chain length, the crossover behavior appears to be common to all semicrystalline polymers investigated so far in our laboratory.

Secondary Crystallization below T_{CO}. We first summarize the experimental observations reported in the Results section. These observations were based on studies of the melting behavior after secondary crystallization. Samples subjected to secondary crystallization below T_{co} exhibit a double-melting behavior. The position and shape of the higher melting endotherm are independent of secondary crystallization time and temperature and are identical to those of partially melted samples. In contrast, the melting temperature associated with the low endotherm increases linearly with the logarithm of time at a rate $B(T_x)$. $B(T_x)$, in turn, decreases linearly with increasing secondary crystallization temperature. The low endotherm location was also found to be approximately independent of primary crystallization conditions, a result already obtained in the case of PEEK.[2,4]

At the early stages of secondary crystallization, log-$[\Delta H_m^{low}]$ increases linearly with log$[t_x]$, the slope (i.e., Avrami exponent) being equal to $^1/_2$. This value of the Avrami exponent was observed at all temperatures below the crossover temperature, regardless of the initial sample morphology. Finally, the magnitude of ΔH_m^{low} appears to depend on the initial level of crystallinity prior to secondary crystallization. We also note that the time dependence of the low endotherm melting

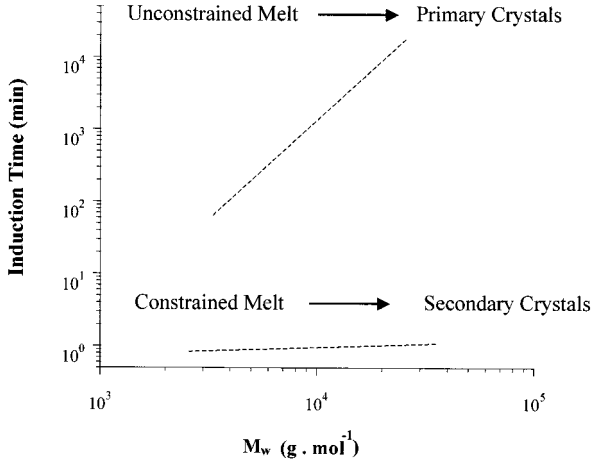

Figure 13. Sketch illustrating the typical induction periods at 190 °C for the formation of primary lamellar crystals and secondary (bundlelike) as a function of the molar mass of BAPC.

temperature is identical for partially melted and original samples if the induction time for the formation of primary crystals is accounted for in original samples.

The general observations presented above are very similar to those reported earlier on the kinetics of secondary crystallization of ethylene/1-octene copolymers and PEEK at low temperatures.[1,2] These results indicate that secondary crystallization of BAPC at $T_x < T_{CO}$ is accounted for by the formation of new crystals. Melting of these secondary crystals takes place in the lower endotherm. We speculate that these crystals are bundlelike or mosaic block structures as they melt (at short times) right above their formation temperature. Our results suggest that the fraction of crystals formed during secondary crystallization is proportional to the fraction of preexisting or primary lamellae (see Figures 5 and 6). Then, it is reasonable to conclude that secondary crystallization is limited to regions in the direct vicinity of primary lamellar crystals. This conclusion further supports our contention that secondary crystallization in the low temperature region involves fairly constrained amorphous chains such as cilia, tie chains, and loose loops.

As anticipated, the slow crystallization kinetics of BAPC makes this polymer a model system for the study of secondary crystallization. In Figure 13, we represent schematically the approximate apparent induction times associated with primary and secondary crystallization below T_{CO} as a function of molar mass. We note that the induction period exhibits a much stronger molar mass dependence for primary lamellar crystals than for secondary crystals. We note without further discussion that the induction time for primary crystallization has the same molar mass dependence as the crystallization half time. We also note that the apparent induction time for secondary crystallization in partially melted samples is about 2−3 orders of magnitude shorter than that required for primary crystallization from a completely free melt. Similar differences are observed for primary and secondary crystallization half times. This large difference in time scales is what has allowed us to distinguish between the various stages of crystallization. In the previous section, we proposed an explanation for the slow kinetics of crystallization of BAPC from an unconstrained melt. Now, we discuss possible reasons for the differences in rates between primary and sec-

ondary crystallization. First, we emphasize that very short induction times for secondary crystal formation seem to be the rule rather than the exception.[1−3] Thus, an account of the differences in induction or half times between primary and secondary crystallization cannot be polymer specific. Second, we recall our inference that secondary crystallization must be initiated in the direct vicinity of preexisting crystals, where the chains are constrained by pinning (cilia, tie-chains, loose loops). The molar conformational entropy of such chain segments is therefore lower than that of the free melt. The driving force toward crystal formation is thus larger for conformationally constrained chains than for chains in the free melt. In other words, at a fixed temperature, a crystal of a given size formed from a conformationally constrained melt will be more stable than that formed from the free melt. Application of classical nucleation theory, then, would suggest that the nucleation rate from a constrained amorphous fraction is larger than from the free melt at the same temperature. It is well-known that such primary nuclei cannot grow significantly in lateral dimensions without the intervention of a chain folding mechanism. While such a mechanism is available for chains in the free melt, it is nonoperative for chains in the direct vicinity of primary lamellae because of the conformational constraints. In conclusion, we anticipate that secondary crystallization is more akin to a sort of primary nucleus (fringe-micelle or chain bundle structure) formation than to lamellar formation, especially when the conformational constraints are significant.[29] In the absence of chain sliding diffusion effects,[30] the above qualitative model provides an explanation for the differences in molar mass dependences of the induction and half times during primary and secondary crystallization. Secondary crystallization is a local phenomenon which only involves a section of a given chain, while primary crystallization, if viewed in the context of the Lauritzen−Hoffman theory, requires biased reptational motion; thus, participation of the whole chain as long as the chain length is not too large.[26]

Before concluding this section, it is pertinent to discuss briefly the secondary crystallization time and temperature dependence of the melting behavior. While a preliminary model was already presented in the two preceding publications and a more general discussion will be given in a forthcoming paper, it suffices to state that we attribute the upward shift of the low endotherm with time, at least partly, to a decrease in the conformational entropy of the remaining amorphous phase as a consequence of bundlelike secondary crystallization.[2,3] The reasoning for this latter statement was in part based on correlated increases in the glass transition and low endotherm melting temperatures with crystallization time for PEEK, PET, and it-PS.[3] Although BAPC does not exhibit a noticeable variation of T_g with time in the course of secondary crystallization, it shows a marked broadening of the width of the glass transition as secondary crystallization proceeds.[15] Considering that BAPC exhibits a significantly lower level of crystallinity, thus a larger fraction of liquidlike amorphous regions as compared to PEEK or PET, the "average" glass transition temperature of BAPC is expected to vary to a lesser degree during the course of crystallization. Hence, the smaller variation of T_g in this case is not inconsistent with the idea of a conformational entropy decrease as a result of secondary crystallization. Indeed, recent modulated DSC experiments by Schick et al.[31] have confirmed that the rigid amorphous fraction in BAPC develops principally as a result of the constraining effects induced by secondary crystals.

Secondary Crystallization above T_{CO}. In the Results section we showed in the case of BAPC-4K and BAPC-28K the existence of a crossover temperature above which a single melting endotherm is observed and the slope $B(T_x)$ increases with crystallization temperature. These trends differ from those observed at lower temperatures, i.e., at $T_x < T_{CO}$. In fact, we believe that secondary crystallization in these two temperature ranges are governed by entirely different mechanisms. It is important to point out that a similar increase of $B(T_x)$ with crystallization temperature above T_{CO} has been observed in our laboratory for other semicrystalline polymers, such as PEEK and it-PS.[3] The increase in the slope $B(T_x)$ with T_x is reminiscent of the behavior observed in linear polyethylene (LPE) samples annealed or isothermally crystallized at temperatures between 124 and 130 °C.[32−35] Furthermore, for LPE, the linear increase in melting temperature with logarithm of time has been unequivocally associated with isothermal lamellar thickening.[33,34] One may wonder if the increase in the slope $B(T_x)$ with crystallization temperature in the case of BAPC has the same physical origin. To examine this possibility we performed AFM experiments on a series of BAPC-28K samples after isothermal annealing at 220 °C. Figure 14a shows a typical set of AFM micrographs after two annealing times. Edge-on parallel lamellae are obtained after both thermal treatments. For a more quantitative analysis, the distributions of lamellar thicknesses were measured from a large number of atomic force micrographs and are represented in Figure 14b. The most probable lamellar thickness shifts toward higher values with annealing time. This result per se provides strong support for the feasibility of isothermal lamellar thickening in BAPC. We note, however, that we were unable to directly correlate the increase in most probable lamellar thickness as obtained from the AFM micrographs with the increment of $B(T_x)$ as determined from DSC measurements. A possible reason for this shortcoming is the significant difference in sample preparation for these two sets of experiments. To determine the distribution of lamellar thicknesses as accurately as possible, lamellar crystals must be imaged edge-on. To achieve this goal, very thin BAPC films were cast from a dilute solution on calcite. After drying and cold crystallization on calcite, lamellar crystals were indeed observed approximately edge-on, possibly as a result of pseudoepitaxy. The samples investigated by calorimetry were bulk crystallized. At this moment we cannot comment on the influences of either the substrate (calcite) or the film thickness on the crystallization behavior of BAPC. Therefore, rather than comparing the data from AFM and DSC studies in absolute terms, we can only conclude that both sets of results are consistent with a mechanism of isothermal lamellar thickening.

We cited earlier that isothermal lamellar thickening is usually thought to be operative in polymers which exhibit an α_C relaxation.[8,9] For such polymers, thickening has been only observed above the so-called $T_{\alpha C}$. We recall that BAPC is generally classified in the group of polymers which lack an α_C relaxation.[10] We note, however, that the dielectric, dynamic mechanical, and even NMR spectroscopic techniques, which are usually employed for the detection of such molecular relaxation,

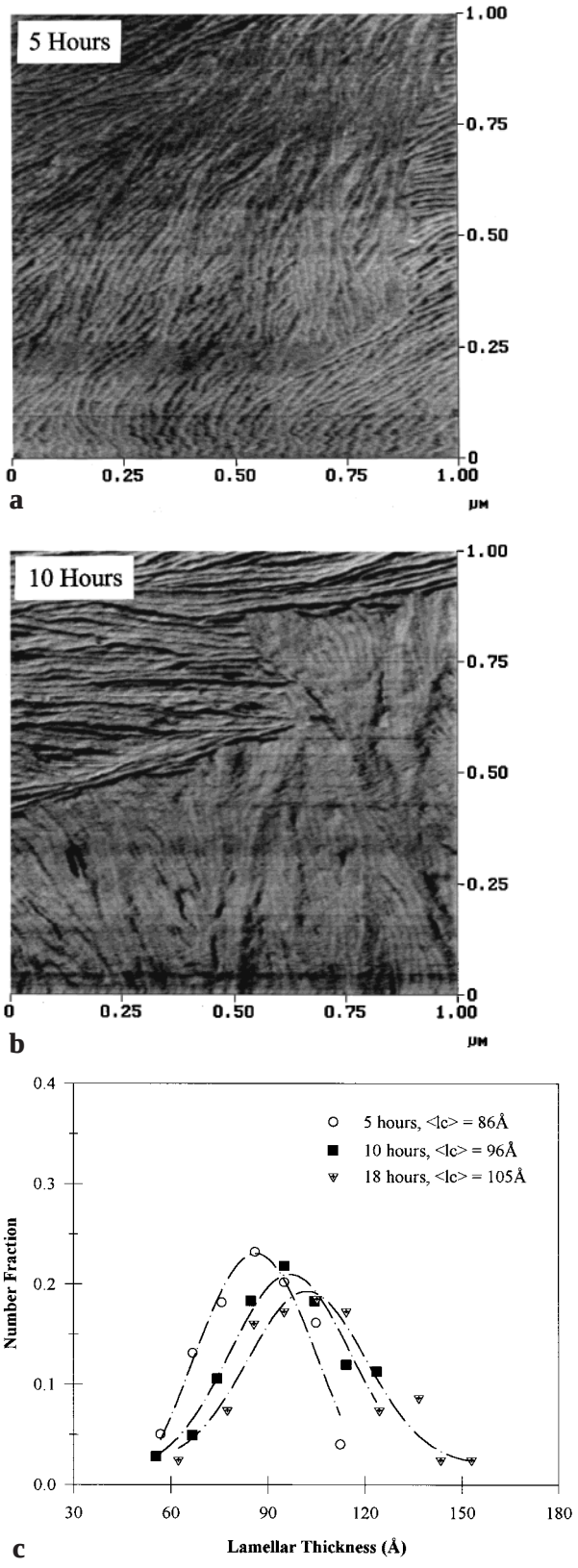

Figure 14. (a) AFM micrographs of BAPC-28K after annealing at 220 °C for 5 and 10 h. (b) Distribution and average lamellar thicknesses of BAPC-28K after annealing at 220 °C for various times.

are usually not employed in the temperature range where significant melting is observed.[10] Our studies suggest that such a relaxation may indeed be present, but at temperatures higher than heretofore investigated. This should not come as a surprise, as at high enough temperatures the crystal lattice may be sufficiently expanded for local chain conformational changes to occur within the crystal phase.

We conclude this section with a proposed explanation for the existence of this crossover phenomenon. First, since isothermal lamellar thickening processes are thermally activated, an increase in $B(T_x)$ with temperature is expected. In polyethylene, for instance, the rate of isothermal lamellar thickening increases with temperature and is only detectable when molecular processes associated with the α_c relaxation are fast enough. Our data would therefore suggest the existence of a link between the crossover temperature and the α_c relaxation. Such a link can also be established from considerations of the decrease of $B(T_x)$ with increasing temperature below T_{co}, which has been extensively discussed in the context of PEEK.[2] As secondary crystallization takes place at increasingly higher temperatures, the resulting morphology evolves from fringe-micellar to mosaic block to lamellar structures. As a consequence of this morphological evolution, the conformational constraints in the remaining amorphous fraction decrease with increasing secondary crystallization temperature. In support of this view, we recall that both T_g and the rate of shift of T_g with time decrease with increasing temperature. Our results[1−3] suggest that $B(T_x)$ is a measure of the magnitude of the constraints, and T_{co}, in turn, would correspond to the temperature where these constraints vanish.

Conclusions

The crystallization rate of BAPC exhibits a very strong molar mass dependence during primary crystallization but not during secondary crystallization. This is explained in terms of mechanistic differences between the primary and secondary stages. The characteristic features of the secondary crystallization process in the low temperature region (i.e., below a well-defined crossover temperature) conform to previous findings in the case of PEEK. Secondary crystallization above the crossover temperature is described in terms of an isothermal lamellar thickening process. Support for the latter assertion is obtained from atomic force microscopy observations. The existence of a crossover phenomenon between secondary crystal formation at low temperature and lamellar thickening at high temperature in the case of BAPC will be extended in a subsequent paper to the case of it-PS, PEEK, and PET. A similar behavior can be inferred from literature data on flexible chain polymers such as linear polyethylene, isotactic poly(propylene) and poly(vinylidene fluoride) and now appears to be possibly a universal feature of polymer crystallization.

Acknowledgment. The authors wish to acknowledge support of this work by the National Science Foundation (NSF Young Investigator Award: DMR 93-57512 and the Science and Technology Center for High Performance Polymeric Adhesives and Composites at VPI&SU: DMR 91-20004).

References and Notes

(1) Alizadeh, A.; Richardson, L.; Xu, J.; McCartney, S.; Marand, H.; Cheung, W.; Chum, S. *Macromolecules* **1999**, *32*, 6221.
(2) Marand, H.; Alizadeh, A.; Farmer, R.; Desai, R.; Velikov, V. *Macromolecules* **2000**, *33*, 3392.
(3) Alizadeh, A.; Sohn, S.; Xu, J.; Elkoun, S.; Marand, H. Manuscript in preparation. Marand, H.; Alizadeh, A. *Proc. Natl. Meet. Am. Chem. Soc., New Orleans* **1999**, *PMSE (81)*, 238.

(4) Velikov, V. Time Dependent Properties of Semicrystalline PEEK above and below the Glass Transition. Ph.D. Dissertation, Virginia Polytechnic Institute & State University, Blacksburg, VA, 1996.
(5) Sohn, S.; Alizadeh, A.; Marand, H. *Polymer* **2000**, *41*, 8879.
(6) Schnell, H. *Chemistry and Physics of Polycarbonates*; Interscience: New York, 1964.
(7) Legras, R.; Mercier, J. P. *J. Polym. Sci., Polym. Phys.* **1979**, *17*, 1171.
(8) Strobl, G. *Physics of Polymers*; Springer-Verlag: Berlin, 1996.
(9) Boyd, R. H. *Polymer* **1985**, *26*, 1123.
(10) Schmidth-Rohr, K.; Hu, W. G. *Acta Polym.* **1999**, *50*, 271.
(11) Schnell, H. *Angew. Chem.* **1956**, *68*, 633.
(12) Sitaramaiah, G. *J. Polym. Sci. Part A* **1965**, *3*, 2743.
(13) Schultz, G. V.; Horbach, A. *Makromol. Chem.* **1959**, *29*, 93.
(14) Berry, G. C.; Nomura, H.; Mayhan, K. G. *J. Polym. Sci., Part A-2* **1967**, *5*, 1.
(15) Sohn, S. Crystallization Behavior of Bisphenol A Polycarbonate: Effects of Crystallization Time, Temperature and Molar Mass. Ph.D. Dissertation, Virginia Polytechnic Institute & State University, Blacksburg, VA, 2000.
(16) Falkai, B.; Rellensmann, W. *Makromol. Chem.* **1964**, *75*, 112.
(17) Falkai, B.; Rellensmann, W. *Makromol. Chem.* **1965**, *88*, 38.
(18) Galez, F.; Legras, R.; Mercier, J. P. *Polym. Eng. Sci.* **1976**, *16*, 276.
(19) Goler, V. F.; Sachs, G. *Z. Phys.* **1932**, *77*, 281.
(20) Wunderlich, B. *Macromolecular Physics*; Academic Press: New York, 1980; Vol. 3.
(21) Marand, H.; Xu, J.; Srinivas, S. *Macromolecules* **1998**, *31*, 8219.
(22) We wish to thank one of the reviewers for bringing to our attention the specific power low exponent. This exponent is unfortunately not easily reconcilable with others available in the literature for various polymers, as it reflects not only the change in spherulitic growth rate and nucleation rate with molar mass but also the influence of molar mass on the Avrami exponent. The latter is especially important here as secondary crystallization processes affect differently the value of the apparent Avrami exponent for different molar masses.
(23) Turska, E.; Pryzgocki, W.; Maslowski, M. *J. Polym. Sci., Part, C.* **1968**, *16*, 3373.
(24) Wissler, G. E.; Crist, B. *J. Polym. Sci., Polym. Phys.* **1980**, *18*, 1257.
(25) Cheng, S. Z. D.; Barley, J. S.; Von Meerwall, D. *J. Polym. Sci., Polym. Phys. Ed.* **1991**, *29*, 515.
(26) Hoffman, J. D.; Miller, R. L. *Polymer* **1997**, *38*, 3151.
(27) Jonza, J. M.; Porter, R. S. *J. Polym. Sci., Polym. Phys.* **1986**, *24*, 2459.
(28) Harron, H. R.; Pritchard, R. G.; Cope, B. C.; Goddard, D. T. *J. Polym. Sci., Polym. Phys.* **1996**, *34*, 173.
(29) Wunderlich, B. *Macromolecular Physics*; Academic Press: New York, 1976; Vol. 2.
(30) Nishi, M.; Hikosaka, M.; Gosh, S.; Toda, A.; Yamada, K. *Polym. J.* **1999**, *31*, 749.
(31) Schick, C.; Wurm, A.; Merzlyakov, M.; Minakov, A.; Marand, H. *Macromol. Symp.* **2001**, *165*, 83.
(32) Fischer, E. W.; Schmidt, G. *Angew. Chem.* **1962**, *74*, 551.
(33) Weeks, J. J. *J. Res. Natl. Bur. Stand. U.S.* **1963**, *A67*, 441.
(34) Stack, G. M.; Mandelkern, L.; Voigt-Martin, I. G. *Polym. Bull.* **1982**, *8*, 421.
(35) Alizadeh, A. Ph.D. Dissertation, UAM, Madrid, 1997.

MA001417S